Research Article

Journal of Molecular Recognition

Received: 28 May 2010, Revised: 15 July 2011, Accepted: 17 July 2011, Published online in Wiley Online Library: 2011

(wileyonlinelibrary.com) DOI: 10.1002/jmr.1158

Structure and elasticity of desmin protofibrils explored with scanning force microscopy

Balázs Kiss[a], Pál Röhlich[b] and Miklós S. Z. Kellermayer[a]*

Desmin filaments form the intermediate filament system of muscle cells where they play important role in maintaining mechanical integrity and elasticity. Although the importance of desmin elasticity and assembly–disassembly dynamics in cellular mechanics is being increasingly recognized, the molecular basis of neither desmin's elasticity nor its disassembly pathway is well understood. In the present work, we explored the topographical structure of purified and reconstituted desmin filaments by using scanning force microscopy. With the addition of divalent cation chelators ethyleneglycoltetraacetic acid or ethylenediaminetetraacetic acid, the filaments disassembled on a time scale of hours to days into stable, thin fibrillar components with variable (up to micrometer) length, smooth surface and uniform thickness, which are identified as protofibrils. Desmin protofibrils appear as elastic structures with a persistence length of 51.5 nm, and their Young's modulus (10.6 MPa) far exceeds that of the mature filament (3.7 MPa). Protofibrillar bundling within the desmin filament results in high longitudinal tensile strength at a large bending flexibility. The stability of protofibrils suggests that desmin may disassemble along a pathway quite distinct from its assembly. Copyright © 2011 John Wiley & Sons, Ltd.

Keywords: desmin; disassembly; protofibril; atomic force microscopy; persistence length

INTRODUCTION

Desmin is the protein building block of intermediate filaments present in every muscle tissue (Bär *et al*., 2004). Intermediate filaments are 8- to 14-nm-thick apolar polymers that form a three-dimensional network in the cytoplasm of metazoan cells (Herrmann and Aebi 2004). Intermediate filament proteins display a common molecular architecture in which a central rod region, composed of four α-helical domains (1A, 1B, 2A, and 2B) interrupted with three linker sequences (L1, L12, and L2), is flanked by head and tail domains (Osborn 1986; Steinert and Parry 1985; Steinert *et al*., 1984). Although similar in the overall structure of their building block, intermediate filaments are quite heterogeneous according to their chemical and assembly properties, which formed the basis of identifying sequence homology classes (SHC) and assembly groups (Herrmann and Aebi 2004; Herrmann and Aebi 2000; Herrmann and Aebi 1999; Kreplak *et al*., 2004; Parry 2005). Desmin together with vimentin and glial fibrillary acidic protein falls in sequence homology class III and assembly group 2. Accordingly, desmin filaments polymerize by the rapid formation of ~58-nm-long unit length filaments (ULFs) (Herrmann and Aebi 2004; Herrmann *et al*., 1999), which are a lateral association of eight tetramers built up from antiparallel, half-staggered coiled-coil dimers (for assembly and disassembly models, see Figure 7). Loosely packed filaments are formed by the longitudinal annealing of ULFs followed by radial compaction in the mature filament (Bär *et al*., 2004; Stromer *et al*., 1987), a process that has been extensively studied by using electron microscopy (EM). At the end of this maturation process, the desmin filament is condensed into a several micrometer-long thread-like structure displaying a diameter of 10 nm on electron micrographs. Under physiological ionic strength and ambient temperature conditions, the assembly of desmin is more or less complete in approximately 2 hr (Herrmann and Aebi 1999; Inagaki *et al*., 1988; Ip and Fellows 1990; Stromer *et al*., 1987). Although the role of the assembly–disassembly dynamics of desmin in cellular mechanics and signaling is increasingly recognized, the exact molecular mechanisms of the disassembly pathway are far from being understood.

Intermediate filaments play fundamental roles in tissue and cell mechanics (Bär *et al*., 2004; Boriek *et al*., 2001; Lazarides 1980; Shah *et al*., 2004; Wang and Stamenovic 2003), although the exact mechanisms of their mechanical function are still unclear. The mechanical role of intermediate filaments is particularly evident in diseases in which the loss of mechanical function and the integrity of various tissues are associated with intermediate filament–protein mutations (Bonifas *et al*., 1991; Munoz-Marmol *et al*., 1998; Omary *et al*., 2004; Pellissier *et al*., 1989). In the muscle, where desmin integrates sarcomeric Z-disks with neighboring Z-disks, mitochondria, cell nucleus, and desmosomes, the knockout of the desmin gene results in the sarcomeric ultrastructural changes and the reduction of active and passive muscle forces (Anderson *et al*., 2002; Balogh *et al*.,

* *Correspondence to: Miklós S. Z. Kellermayer, Department of Biophysics and Radiation Biology, Faculty of Medicine, Semmelweis University, Tűzoltó u. 37–47, Budapest H-1094, Hungary.*
E-mail: miklos.kellermayer@eok.sote.hu

a *B. Kiss, M. S. Z. Kellermayer*
Department of Biophysics and Radiation Biology, Faculty of Medicine, Semmelweis University, Tűzoltó u. 37-47, Budapest H-1094, Hungary

b *P. Röhlich*
Department of Human Morphology and Developmental Biology, Semmelweis University, Faculty of Medicine, Tűzoltó u. 58, Budapest H-1094, Hungary

Abbreviations: *AFM, atomic force microscopy; ULF, unit length filament; EGTA, ethyleneglycoltetraacetic acid; EDTA, ethylenediaminetetraacetic acid.*

2005; Lacolley *et al.*, 2001; Sam *et al.*, 2000; Sjuve *et al.*, 1998). Desmin is likely to play an important role in sarcomeric force transmission via its tethering function (Meyer *et al.*, 2010). Not all of the desmin gene mutations affect its polymerization ability (Sharma *et al.*, 2009), but the arginine-rich non-α-helical head domain seems to be absolutely required for proper desmin polymerization. Mutations involving conservative sequences in desmin head domain result in distorted protein assembly already in ULF stage (Sharma 2009). Central rod mutations lead to entangled filaments showing apparent signs of protein aggregation and impaired tensile properties compared with the wild-type desmin (Kreplak *et al.*, 2008).

Only few investigations have dealt with the mechanical properties of intermediate filaments at the single-filament level, and the details of the intrafilamental structural changes that might be responsible for their viscoelasticity are yet unresolved. Rheology measurements on bulk samples indicated that in contrast to microtubules and microfilaments that rupture when exposed to shear stress, intermediate filaments display viscoelastic behavior that manifests in strain hardening (nonlinear elasticity) and yield (stress relaxation) (Janmey *et al.*, 1991; Ma *et al.*, 1999). Mechanical measurements on hagfish slime threads, which contain packed and oriented intermediate filaments, revealed a pronounced elasticity (up to 34% strain) and that mechanical yield may involve a conformational transition from α to β (Fudge *et al.*, 2003). The measurement of orientation distribution along the contour of surface-equilibrated vimentin filaments with atomic force microscopy (AFM) provided an estimate of ~1 μm for the persistence length of intermediate filaments (Mücke *et al.*, 2004). The investigation of the mechanical properties of desmin, keratin, and neurofilaments in experiments where individual surface-attached filaments were stretched by a forced lateral movement of the AFM tip (Kreplak *et al.*, 2005) resulted in a filament tension value of several nanonewtons (calculated for the total filament cross section). The evoked morphological changes revealed that the filaments are highly elastic and can be stretched up to 3.4-fold at the expense of a reduction in filament diameter and height (Kreplak 2008). Exploring the nanomechanics of desmin by manipulating individual filaments with AFM resulted in complex, hierarchical force responses, including an initial unbinding transition that corresponds to the removal of approximately 45-nm-long coiled-coil dimers from the filament surface with 20- to 60-pN forces in usually two discrete steps (Kiss *et al.*, 2006). However, the exact structural rearrangements underlying desmin elasticity remain elusive.

In the present work, we studied surface-adsorbed desmin filaments with AFM. Desmin filaments treated with the divalent cation chelators ethyleneglycotetraacetic acid (EGTA) or ethylenediaminetetraacetic acid (EDTA) were disassembled using a fraying mechanism into stable fibrillar structures identified here as protofibrils. Shape fluctuation analysis allowed us to describe the elastic properties of desmin protofibrils and to compare their behavior to that of mature filaments.

MATERIALS AND METHODS

Purification of desmin

Desmin was handled as described previously (Kiss *et al.*, 2006). Briefly, desmin was purified from chicken gizzard under denaturing conditions, after a tissue extraction with potassium iodide (KI) (Geisler and Weber 1980). Combined desmin-rich fractions were stored in 6 M of urea on ice for up to 6 months, without freezing and without noticeable degradation or loss of polymerization ability. Already polymerized desmin filaments were stable at room temperature for several weeks without showing fragmentation or degradation. Samples used for more extended times were stored at 4 °C. Purity was checked with densitometry of sodium dodecyl sulfate (SDS)–polyacrylamide gel electrophoretogram (PAGE). Protein identity was analyzed with Western blot using antihuman desmin having cross reactivity with chicken desmin (clone D33; Dako, Denmark). Typical purification procedures yielded a desmin of high purity (more than 97%), with a concentration of approximately 0.8 mg/ml on the basis of gel densitometry and spectrophotometry (Kiss *et al.*, 2006). Upon assembly initiation (see the next section), the samples were slightly diluted to a final concentration of ~0.67 mg/ml.

Reconstitution and treatment of desmin filaments

Desmin filaments were reconstituted by the removal of denaturant and the addition of salt. Small aliquots were dialyzed against 10 mM of Tris–HCl (pH 8.0, 4 °C, 3× 2 h), then against 1 mM of $NaHCO_3$ (pH 8.0, 4 °C, 3× 2 h). Protein aggregates were removed by ultracentrifugation (100 000×*g*, 30 min, 4 °C) and filtration (0.22 μm membrane filter; Millipore, Bedford, MA). Filament reconstitution was initiated by the addition of imidazole (pH 7.0, 5 mM final concentration) and $MgCl_2$ (2 mM final concentration). The dilution of desmin samples, if necessary, was carried out with buffer containing the previously mentioned constituents ("dilution buffer"). Aggregated filament entanglements were dispersed by the addition of Triton X-100 to a final concentration of 0.1%. Occasionally, desmin filaments were rejuvenated by a cycle of denaturation (dialysis against 6 M urea, pH 7.5, 4 °C, for 2 h) and renaturation (dialysis and polymerization as previously mentioned).

To disrupt desmin filaments, samples were exposed to high concentrations of either 40 mM of EGTA or 16 mM of EDTA. Typical incubation times ranged between 2 hr and 21 days. Nonspecific protein degradation was not detectable with SDS–PAGE.

Atomic force microscopy

For AFM measurements, desmin filaments were attached to freshly cleaved mica. An aliquot of desmin (10–20 μl) was pipetted onto the mica surface and incubated at room temperature for 10 min. Unbound fibrils were washed away by rinsing extensively with distilled water then by blowing gently with a stream of high-purity N_2 gas.

The noncontact mode (alternating current or AC mode) AFM images of desmin filaments bound to mica surface were acquired with an MFP3D AFM instrument (Asylum Research, Santa Barbara, CA). Scanning was performed at high set-point values (0.8–1.2 V) to avoid the binding of the sample to the cantilever tip. Silicon–nitride cantilevers (Olympus) were used for scanning in air (AC160TS, resonance frequency ~300 kHz). At a typical scanning frequency of 0.7–1.4 Hz, we collected 512 × 512-pixel or 1024 × 1024-pixel height-, amplitude-, and phase-contrast images.

Electron microscopy

For EM, we used desmin samples at a protein concentration of 25–50 μg/ml. Samples were added to glow-discharged carbon-coated grids, negatively stained with 1% uranyl acetate and visualized by using a Hitachi 7100 transmission electron microscope

Journal of Molecular Recognition

at an accelerating voltage of 80 kV and with a typical magnification of 60 000–80 000.

Image analysis

Images were edited and analyzed using the MFP3D (Asylum Research) built-in routines of Igor Pro 6.04 (Wavemetrics, Lake Oswego, OR). Statistical analyses were carried out by using KaleidaGraph (version 4.0.2; Synergy Software, Reading, PA). The local topography of filaments was obtained by scanning with the free-hand tool along the filament axis. The autocorrelation function was calculated with the built-in algorithms of IgorPro. Average filament height (h) was obtained by measuring the distance between the height data along the filament axis and the background height values. Actual filament width (w) was calculated from the apparent filament width (A), measured as the full width at half maximum on the cross-sectional profile plot, by correcting for tip geometry (see Figure 3c):

$$w = A - 2c \tag{1}$$

where c is a correction factor calculated as

$$c = \sqrt{2rh - h^2} \tag{2}$$

where r is the tip radius (9 ± 2 nm for the used AC160TS cantilever according to Olympus factory specifications) and h is the measured average filament height.

The persistence length (P, measure of bending rigidity) of desmin filaments and protofibrils was assessed by analyzing the relationship between the end-to-end distance (R) and the contour length (L) of surface-equilibrated filaments as (Rivetti *et al*., 1996):

$$\langle R^2 \rangle_{2D} = 4PL\left(1 - \frac{2P}{L}\left(1 - e^{-\frac{L}{2P}}\right)\right) \tag{3}$$

Persistence length can be related to the macroscopic quantities of Young's modulus (E) and area moment of inertia (I) as

$$P = \frac{EI}{k_B T} \tag{4}$$

where k_B is the Boltzmann's constant (1.38×10^{-23} JK^{-1}) and T is the absolute temperature (300 K, room temperature). For a beam with circular cross section, such as the desmin filament, the area moment of inertia is

$$I = \frac{\pi d^4}{64} \tag{5}$$

where d is filament diameter (10 and 4.5 nm for desmin filaments and protofibrils, respectively) (Aebi *et al*., 1983).

RESULTS

Morphology of desmin

Reconstituted desmin filaments adsorbed to mica appeared as curved, bent filaments with lengths up to several microns (Figure 1a). Filaments appeared already 30 min after the initiation of polymerization by the addition of salt (usually $MgCl_2$), and they remained stable for several weeks. In some cases, we investigated rejuvenated filaments that were repolymerized after an additional cycle of denaturation with urea. We could observe no morphological differences between the old and the rejuvenated desmin filaments. Often the filaments formed entanglements (Figure 1a.i), which could be dispersed by the addition of 0.1% Triton X-100. The surface-adsorbed dried filaments usually displayed a beaded, segmented structure (Figure 1a.ii).

Upon treating the desmin filament sample with either EDTA (16 mM) or EGTA (40 mM), thin fibrillar structures appeared beside mature filaments (Figure 1b). Mature filaments were embedded in a meshwork of these thin fibrils (Figure 1b.i). In a diluted sample, the thin fibrils appeared as distinct entities with uniform thickness, smooth surface, and highly variable length (Figure 1b.ii). Occasionally, thin fibrils up to a micrometer in length were observed. Short thin fibrils appeared already after 1 day in the case of treatment with EDTA. By contrast, in the case of EGTA, a week-long incubation was necessary to evoke the appearance of the thin fibrils, which appeared longer than that in the case of EDTA treatment. Sometimes the transition from the mature filament to the thin fibrils could be observed (Figure 1c). c). In such cases, usually the ends of the filaments were frayed, and two to four thin fibrils appeared at the filament end. To test whether the extended treatment may have caused protein degradation, we carried out SDS–PAGE. An example SDS–PAGE of a desmin sample treated for 9 days with 40 mM of EGTA is shown in Figure 1d. We observed no sign of protein degradation, which would have manifested in a smeared band.

Analysis of axial topography

The topographical height along the axis of individual desmin filaments and thin fibrils was measured using height profile plots (Figures 2a and 2b). Height varied significantly along the axis of mature filaments (Figure 2a, top). A range (difference between maximum and minimum height) of up to 4.751 nm was observed. The variance of topographical height was 0.607 nm^2. By contrast, the topography of the thin fibrils appeared much smoother (Figure 2b), with a height variance of only 0.003 nm^2. In the axial topography of mature fibrils, periodic peaks and valleys could be discerned. The autocorrelation analysis of the topographical height (Figure 2a, bottom) revealed the periodic nature of height variation. The analysis of 358 periods in 30 desmin filaments resulted in a broad, multimodal distribution (Figure 2c) with a mean period of 105.25 nm (SD = 47.28 nm). Notable peaks in the periodicity histogram are at approximately 60 and 120 nm, which are the integer multiples of the lengths of the ULF (Kreplak *et al*., 2004).

Analysis of global dimensions

The average topographical height of mature desmin filaments and thin fibrils (called tentatively in the figures as *protofibrils*) are shown in Figure 3a. The height of mature filaments is relatively broadly distributed around a mean of 2.32 nm (SD = 0.40 nm, $n = 87$). The histogram of mean thin fibril height displays a Gaussian distribution (Figure 3a, inset) with a mean of 0.30 nm (SD = 0.05 nm, $n = 101$).

The apparent width (A) of filaments and thin fibrils is shown in Figure 3b. Mature filaments have an average apparent width of 62.63 nm (SD = 6.71 nm, $n = 38$), whereas thin fibrils have an average width of 30.05 nm (SD = 3.76 nm, $n = 44$). The real width (w)

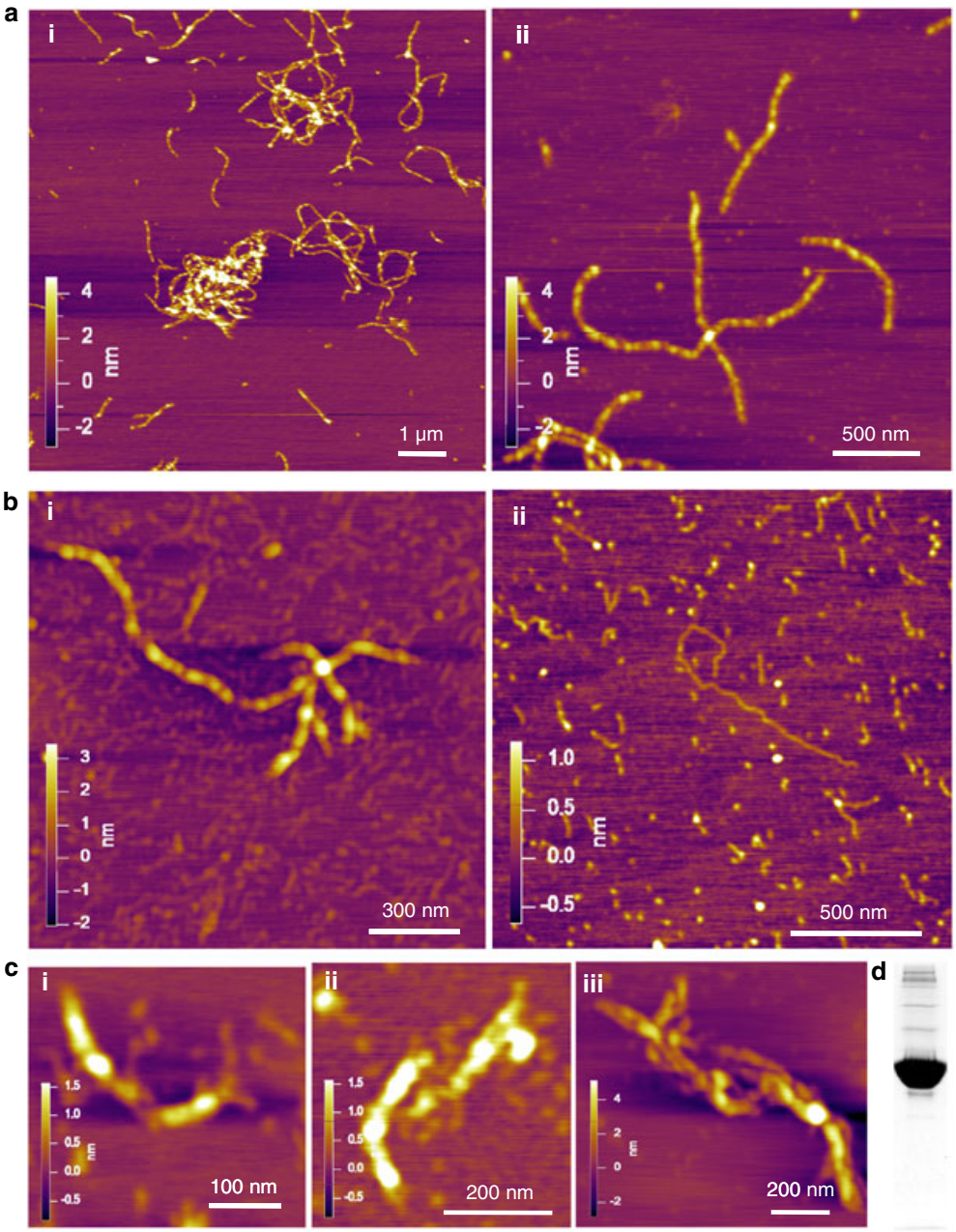

Figure 1. Scanning force microscopic morphology of desmin. (a) Desmin filaments adsorbed to freshly cleaved mica, washed with distilled water, dried, and then imaged in air. (i) Large field of view displaying a mixture of individual and entangled filaments. (ii) Enlarged view displaying subfilamentous structural detail. (b) Thin fibrillar structures after the treatment of the desmin sample with 40 mM of EGTA for nine days. (i) Concentrated sample displaying a filament in a meshwork of thin fibrils (protofibrils). (ii) Sample diluted 50-fold with "dilution buffer" (see Materials and Methods). (c) (i–iii) AFM images of desmin filaments unraveling into thin fibrils (protofibrils). (d) Overloaded SDS–PAGE gel stained with Coomassie blue of a desmin sample treated with 40 mM of EGTA for 9 days.

was calculated by taking into account the geometry and the dimensions of the AFM cantilever tip (Figure 3c) and by calculating a corresponding correction factor (*c*) according to **Equation (2)**. The calculated real width of mature desmin filaments is 50.60 nm, and that of thin fibrils is 25.52 nm. Considering the width-to-height ratios, both mature filaments and thin fibrils are significantly flattened on the mica surface compared with an expected circular cross section. Assuming a flattened rectangular cross-sectional shape, the circumference can be calculated from the height and real width data. The circumference of mature desmin filaments is 105.84 nm, which corresponds to a diameter of 33.68 nm for a cylindrical filament. Thus, taking the electron microscopically characterized 10-nm diameter of mature desmin filaments into account (Stromer *et al*., 1981), there is an approximately 3.4-fold increase in the cross-sectional dimensions of the filaments, which probably occurred because of the different sample preparation (e.g., surface adsorption, dehydration) of AFM measurement in contrast to the one of the EM. The circumference of thin fibrils is 51.62 nm, which corresponds to a diameter of 16.44 nm for a cylindrical fibril. Assuming a similar, 3.4-fold increase

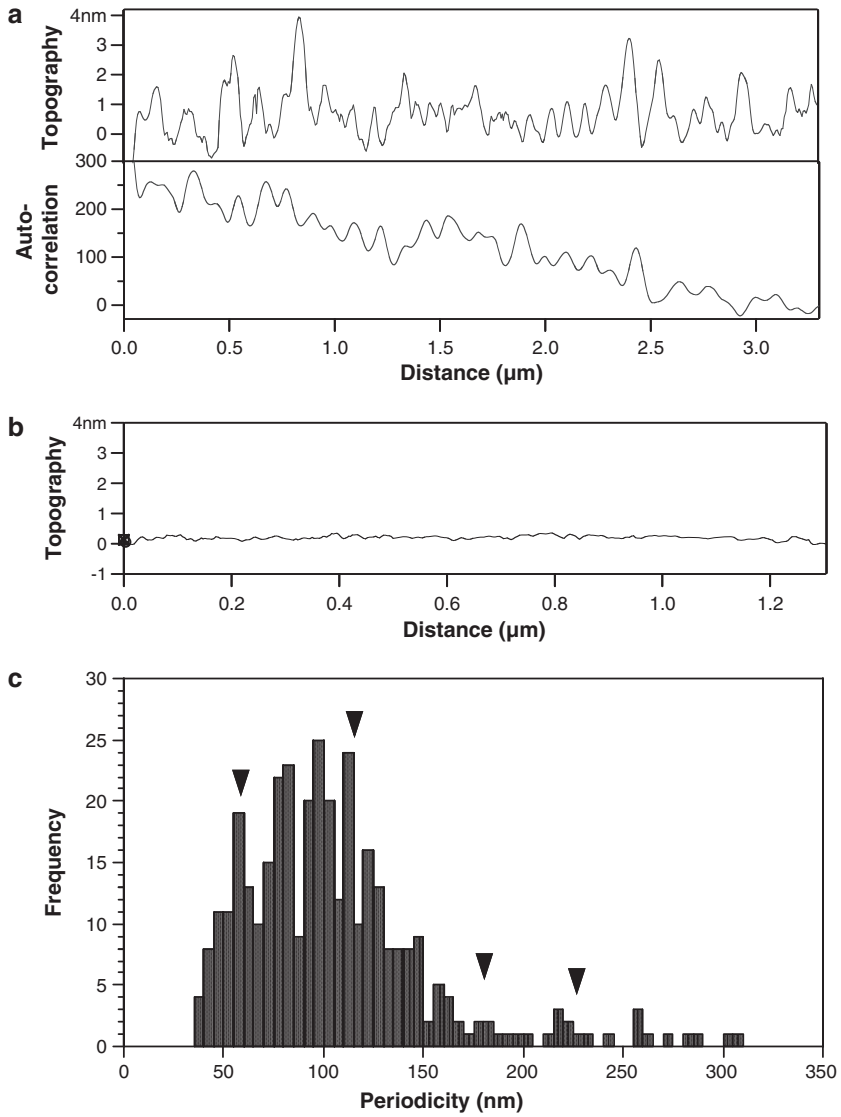

Figure 2. Analysis of the topography of desmin filaments and protofibrils. (a) Topographical height fluctuations along the axis of a single desmin filament (top). The average height was subtracted from the local height values. The autocorrelation function of the height fluctuations (bottom). (b) Topographical height distribution along the axis of a single desmin protofibril. Axis scaling was identical to that of the desmin filament (panel a, top) so as to compare the magnitude of fluctuation in the data. (c) Distribution of the distances separating consecutive peaks in the autocorrelation function of the topographical height of desmin filaments. Arrowheads refer to the integer multiples of ULF dimensions.

in cross-sectional dimensions, the true diameter of the thin fibrils is approximately 4.83 nm, a value similar to the diameter of keratin protofibrils (Aebi *et al*., 1983). To verify the calculated width of desmin filaments and thin fibrils, we performed EM experiments (Figure 4). The analysis of mature desmin filaments resulted in an average diameter of 10.3 nm (Figures 4a and 4b), which is comparable with the electron microscopic reference diameter of mature filaments used to determine the increment factor for AFM analysis. Thin fibrils had an average diameter of 4.1 nm (Figures 4c and 4d) on the basis of the electron micrographs.

The contour-length distribution of thin fibrils obtained after either EGTA or EDTA treatment is shown in Figure 5. Multimodal distributions are seen with mean contour lengths of 143.14 nm (SD = 56.10 nm, $n = 279$) and 87.05 (SD = 36.70, $n = 31$) for EGTA- and EDTA-treated fibrils, respectively. Notable peaks, seen in the EGTA-treated fibrils, occur at approximately 60, 120, and 180 nm, which correspond to the integer multiples of the ULF dimensions (Kreplak *et al*., 2004).

Analysis of elasticity

The parameters of filament and thin fibril elasticity were obtained by analyzing their global shape in terms of contour length and end-to-end distance. The results are shown in Figure 6. Fitting **Equation (3)** to the mean square end-to-end distance versus contour length functions resulted in persistence lengths of 432.6 nm (SD = 4.2 nm, error of fit) and 51.5 nm (SD = 0.7 nm, error of fit) for desmin filaments and thin fibrils, respectively. The Young's moduli of desmin filaments and thin fibrils were calculated according to **equation 4** using the obtained persistence length data and the area moments of inertia **(equation 5)** for mature desmin filaments and 4.5-nm protofibrils (Aebi *et al*.,

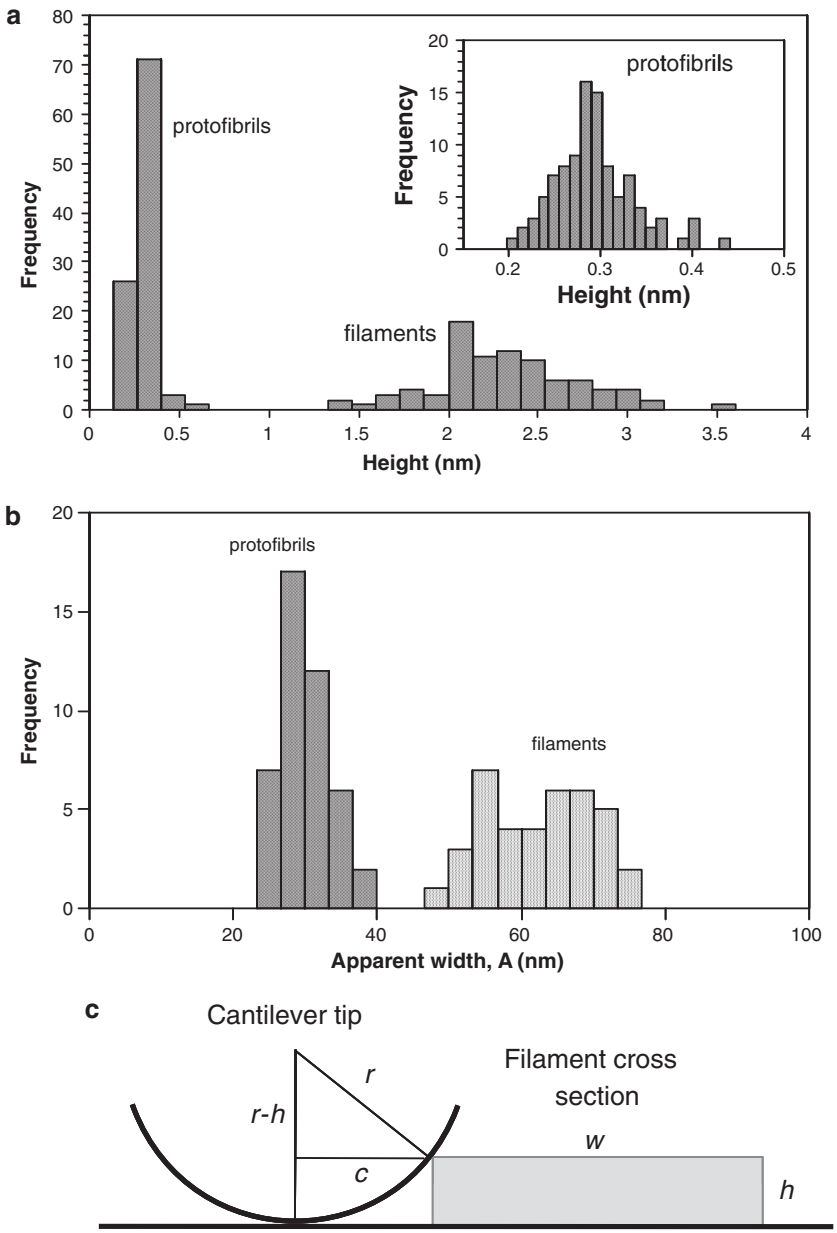

Figure 3. Height analysis of desmin filaments and protofibrils. (a) Distribution of the average topographical height of desmin filaments and protofibrils. (Inset) Detailed protofibril height histogram. (b) Distribution of the apparent width of desmin filaments and protofibrils. (c) Schematics of calculating the real width (*w*) of filaments or protofibrils from the height (*h*), cantilever tip radius (*r*), and a correction distance (*c*) related to tip convolution.

1983). The calculated Young's moduli are 3.7 and 10.6 MPa for desmin filaments and thin fibrils (tentatively protofibrils), respectively.

DISCUSSION

The properties of purified desmin intermediate filaments were analyzed in the present work by using scanning force microscopy. Although AFM is a versatile tool for studying biomolecules with sub-nanometer accuracy, the specificities of sample preparation and the distinct mode of operation may result in differences of geometric parameters when compared with EM. Therefore, we also performed EM measurements on our samples. Filaments adsorbed to mica surface were significantly flattened (width-to-height ratio approximately 25). The similar broadening of filament width has been observed for desmin in AFM images (Kreplak *et al.*, 2008). We attribute the flattening and broadening to sample preparation (adsorption to mica, dehydration). It is not inconceivable, however, that swelling and partial structural unraveling have taken place before the adsorption of the filaments to the surface, considering the approximately 3.4-fold increase in cross-sectional dimensions (see Figure 3). In the axial topographical height, a periodic fluctuation was observed (Figure 1a), and autocorrelation analysis has revealed distinct periodicities (Figure 2). The beaded or segmented structure of intermediate filaments has been observed before in AFM (Kreplak *et al.*, 2005) and electron microscopy (Aebi *et al.*, 1983; Milam and Erickson 1984) measurements. The 105-nm average periodicity observed here may be related to the helical twist of

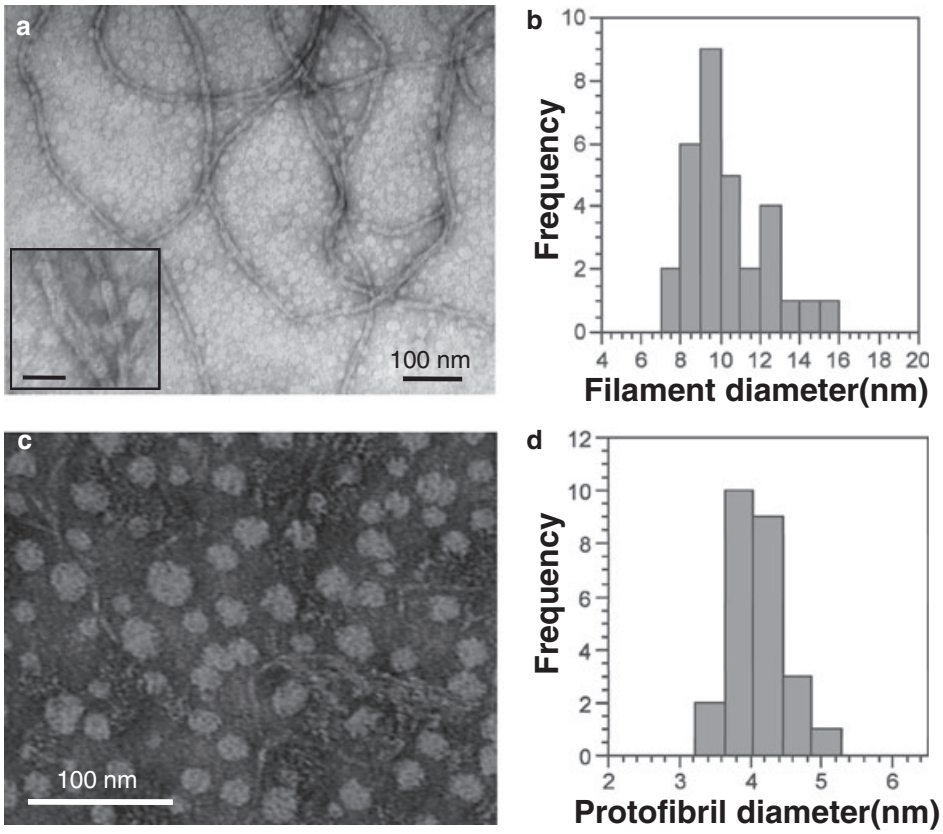

Figure 4. EM analysis of desmin. (a) Negatively stained electron micrograph showing mature desmin filaments. The spherical "champaigning" artifacts emerged randomly but did not interfere with the width analysis. (Inset) Enlarged view of a filament partially frayed into component protofibrils. Scale bar, 20 nm. (b) Filament width histogram. (c) Negatively stained electron micrograph showing desmin protofibrils. The spherical "champaigning" artifacts emerged randomly but did not interfere with the protofibril width analysis. (d) Protofibril width histogram.

underlying fibrillar structures or to the partially overlapping structural units (tetramers or ULFs) (Kreplak *et al*., 2004). We observe that the periodicity is relatively widely distributed. It is an intriguing possibility that the periodicity may change with the mechanical state (bending and stretching) of the filament and hence correspond to the structural rearrangements underlying filament elasticity.

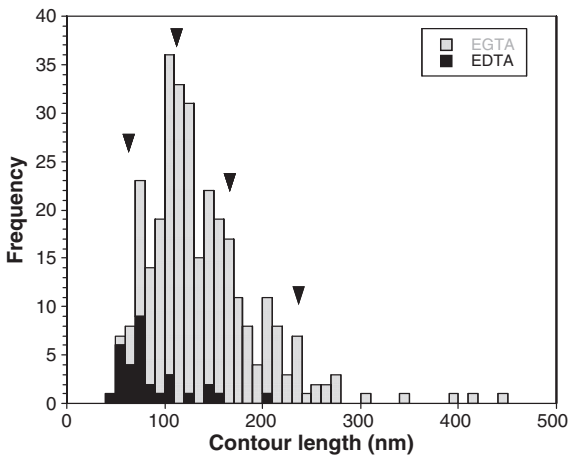

Figure 5. Contour length distribution of desmin protofibrils prepared with either EDTA or EGTA treatment of the desmin filament sample. Arrowheads refer to the integer multiples of ULF dimensions.

Upon the treatment of desmin filaments with the divalent cation chelators EDTA or EGTA, they unraveled into fibrillar structures of variable length but uniform thickness and surface smoothness. EDTA treatment resulted in a rapid fraying of mature desmin filaments into very short fibrils (Figure 5). By contrast, the frequency of long filaments was much greater in the EGTA-treated sample. A peak at ~60 nm can be identified for both EDTA- and EGTA-treated samples, suggesting a similar fundamental building block (ULF) for fibrils disassembled with either chelator. The effect is possibly more rapid and prominent in the case of EDTA, presumably because of its higher affinity to Mg^{++} ions used to evoke desmin polymerization. It has been previously shown that calcium-binding proteins (S-100 family) stimulate the disassembly of desmin (Garbuglia *et al*., 1996), but along an unresolved molecular pathway. On the basis of the number of fibrillar structures per filament (two to four; Figure 1c) and the cross-sectional dimensions measured and calculated on AFM images (Figure 3) and electron micrographs (Figures 4c and 4d), we hereby identify them as desmin protofibrils. The protofibril diameter calculated from the AFM images (4.83 nm) and measured on electron micrographs (4.1 nm) are comparable, lending support to the validity of the shape-correction calculations **(equation 2)** and to the identity of the thin fibrillar structures. Desmin protofibrils, as observed here, are distinct structural entities that are stable in isolation. The protofibrillar

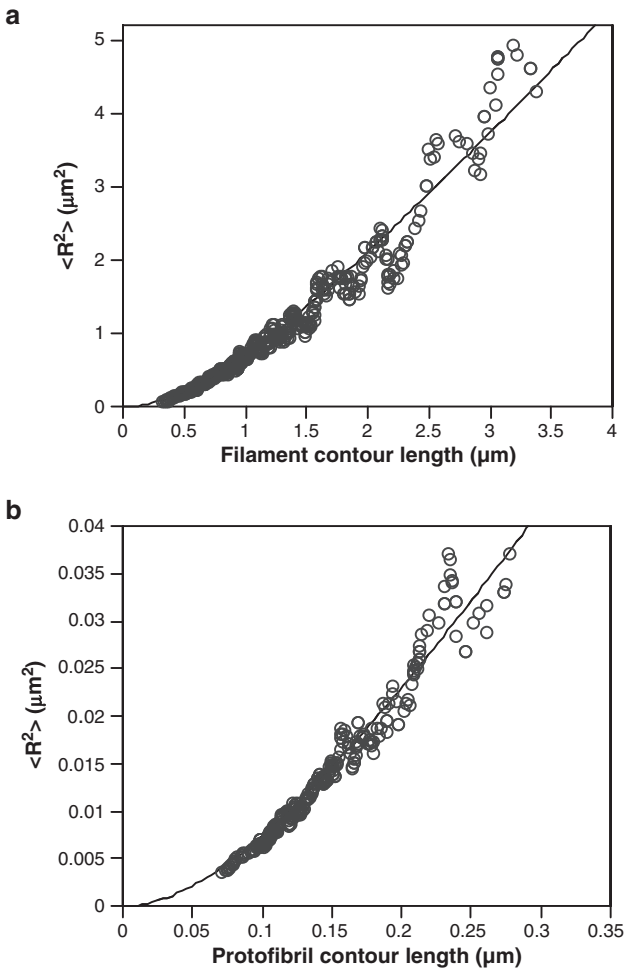

Figure 6. Calculation of filament elastic parameters on the basis of the analysis of shape. Mean square end-to-end distance versus contour length functions of desmin filaments (a) and protofibrils (b). Fits are according to Equation (3). *R*-values of the fits were 0.98 in both cases.

structure underlying intermediate filaments has been demonstrated before (Aebi *et al*., 1983), and desmin filaments have been shown to disassemble into 2-nm protofilaments upon denaturant treatment (Stromer *et al*., 1981). Protofibrils seen here are most likely formed of the parallel bundles of protofilaments, but the current resolution was insufficient to reveal further structural detail. The existence of protofibrils as distinct structural elements suggests that the interactions stabilizing them longitudinally are stronger than the ones connecting them laterally within the filament (Figure 7). The interactions that bind the protofibrils together in the desmin filament are most likely electrostatic and modulated by divalent cations, given the observation that EDTA and EGTA evoked the unraveling process.

Desmin protofibrils are elastic structures as indicated by the analysis of their global shape (Figure 6). Their persistence length is 51.5 nm on the basis of the average shape of surface-equilibrated protofibrils. The persistence length value calculated here compares well with the length of the desmin dimer (Milam and Erickson 1984), suggesting that the structural composition of the protofibril is manifested in its entropic elasticity, and protofibrils may be considered as a statistical chain of serially connected segments with a size that of the dimer. The Young's modulus of the 4.5-nm-diameter desmin protofibril is a factor of 3, greater than that of the mature filament. If the filament were homogenous and isotropic, then a protofibril of identical material properties but about one half of the filament diameter would be much more flexible. In the same logic, if the desmin filament were simply an enlarged version of the protofibril carrying the protofibril's material properties, then the filament would be three times stiffer. The desmin filament is therefore more flexible than expected on the basis of the elastic properties of the underlying protofibril. The increased flexibility most likely stems from the fact that the interactions holding the protofibrils together laterally are weaker than the ones stabilizing them in the longitudinal direction. Our observation of the fraying at the ends of desmin filaments into protofibrils supports this idea.

Desmin has been previously shown to assemble via an end-to-end annealing of ~60-nm-long ULFs, which are structural elements containing the entire cross-sectional composition of the mature filament (Bär *et al*., 2004; Herrmann and Aebi 2004; Herrmann *et al*., 1999; Kreplak *et al*., 2004) (Figure 7). Protofibrils have not been shown along the assembly pathway of desmin or other cytoplasmic intermediate filaments. After the interconnection of ULFs, a maturation process takes place, which involves the formation of inter- and intramolecular cross-links that result in the compaction of the filament and the decrease of filament diameter (Herrmann and Aebi 2004; Kreplak *et al*., 2004; Stromer *et al*., 1987). The observation here of stable desmin protofibrils suggests that filament disassembly may follow a pathway quite distinct from that of the assembly process (Figure 7). The cross-links formed during filament maturation most likely stabilize the underlying fibrillar elements in axial direction, resulting in high longitudinal tensile strength while maintaining a high bending flexibility. Although the appearance of individual protofibrils upon chelator treatment is rather slow (hours to days), it is not inconceivable that *in vivo* mechanisms may significantly accelerate the process. Should such a disassembly process occur, it is likely to take place via fraying at either filament end.

CONCLUSIONS

Purified, surface-adsorbed desmin intermediate filaments were investigated here by using scanning force microscopy. The treatment of desmin with the divalent cation chelators EGTA or EDTA resulted in the fraying and disassembly of mature filaments into distinct, stable fibrillar structures identified as protofibrils. The appearance of distinct protofibrils suggests that the disassembly pathway of desmin may be quite different from its assembly pathway. Desmin protofibrils are elastic with a persistence length of 51.5 nm. Within the mature filament, the interactions stabilizing the protofibril axially are stronger than the ones interconnecting them laterally, providing the filament with large longitudinal tensile strength at large bending flexibility.

Acknowledgements

This work was supported by grants from the Hungarian Science Foundation (OTKA K73256 and K84133), the Hungarian National Office of Research and Technology (NANOAMI KFKT-1-2006-0021, OMFB-380/2006), the Hungarian Medical Research Council (ETT-229/09), and the Hungarian National Development Agency (TAMOP-4.2.1.B-09/1/KMR-2010-0001).

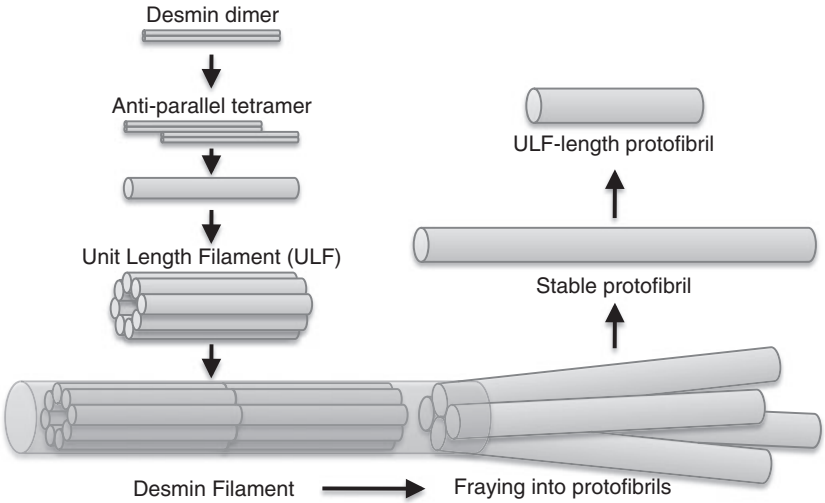

Figure 7. Desmin filament assembly and disassembly pathway. Mature filament composes of several longitudinally annealed ULFs. Protofibrils are stable disassembly intermediates, indicating that longitudinal stability is possibly stronger than lateral.

REFERENCES

Aebi U, Fowler WE, Rew P, Sun TT. 1983. The fibrillar substructure of keratin filaments unraveled. *J. Cell Biol.* **97**(4): 1131–43.

Anderson J, Joumaa V, Stevens L, Neagoe C, Li Z, Mounier Y, Linke WA, Goubel F. 2002. Passive stiffness changes in soleus muscles from desmin knockout mice are not due to titin modifications. *Pflugers Arch.* **444**(6): 771–6.

Balogh J, Li Z, Paulin D, Arner A. 2005. Desmin filaments influence myofilament spacing and lateral compliance of slow skeletal muscle fibers. *Biophys. J.* **88**(2): 1156–65.

Bär H, Strelkov SV, Sjöberg G, Aebi U, Herrmann H. 2004. The biology of desmin filaments: how do mutations affect their structure, assembly, and organisation? *J. Struct. Biol.* **148**: 137–152.

Bonifas JM, Rothman AL, Epstein EH. 1991. Epidermolysis bullosa simplex: evidence in two families for keratin gene abnormalities. *Science* **254**: 1202–1205.

Boriek AM, Capetanaki Y, Hwang W, Officer T, Badshah M, Rodarte J, Tidball JG. 2001. Desmin integrates the three-dimensional mechanical properties of muscles. *Am. J. Physiol.* **280**: C46-C52.

Fudge DS, Gardner KH, Forsyth VT, Riekel C, Gosline JM. 2003. The mechanical properties of hydrated intermediate filaments: insights from hagfish slime threads. *Biophys. J.* **85**(3): 2015–27.

Garbuglia M, Verzini M, Giambanco I, Spreca A, Donato R. 1996. Effects of calcium-binding proteins (S-100a(o), S-100a, S-100b) on desmin assembly in vitro. *FASEB J.* **10**(2): 317–324.

Geisler N, Weber K. 1980. Purification of smooth-muscle desmin and a protein-chemical comparison of desmins from chicken gizzard and hog stomach. *Eur. J. Biochem.* **111**(2): 425–33.

Herrmann H, Aebi U. 2004. Intermediate filaments: Molecular structure, assembly mechanisms, and integration into functionally distinct intracellular scaffolds. *Annu. Rev. Biochem.* **73**: 749–789.

Herrmann H, Häner M, Brettek M, Ku N-O, Aebi U. 1999. Characterization of distinct early assembly units of different intermediate filament proteins. *J. Mol. Biol.* **286**: 1403–1420.

Herrmann H, Aebi U. 2000. Intermediate filaments and their associates: multi-talented structural elements specifying cytoarchitecture and cytodynamics. *Curr Op Cell Biol* **12**:79–90.

Herrmann H, Aebi U. 1999. Intermediate filament assembly: temperature sensitivity and polymorphism. *Cell. Mol. Life Sci.* **55**: 1416–1431.

Inagaki M, Gonda Y, Matsuyama M, Nishizawa K, Nishi Y, Sato C. 1988. Intermediate filament reconstitution in vitro. The role of phosphorylation on the assembly-disassembly of desmin. *J. Biol. Chem.* **263**(12): 5970–8.

Ip W, Fellows ME. 1990. Fluorescent measurement of desmin intermediate filament assembly. *Anal. Biochem.* **185**(1): 10–6.

Janmey PA, Euteneuer U, Traub P, Schliwa M. 1991. Viscoelastic properties of vimentin compared with other filamentous biopolymer networks. *J. Cell Biol.* **113**(1): 155–60.

Kiss B, Karsai Á, Kellermayer MSZ. 2006. Nanomechanical properties of desmin intermediate filaments. *J. Struct. Biol.* **155**(2): 327–339.

Kreplak L, Bär H, Leterrier JF, Herrmann H, Aebi U. 2005. Exploring the mechanical behavior of single intermediate filaments. *J. Mol. Biol.* **354**: 569–577.

Kreplak L, Herrmann H, Aebi U. 2008. Tensile properties of single desmin intermediate filaments. *Biophys. J.* **94**: 2790–2899.

Kreplak L, Aebi U, Herrmann H. 2004. Molecular mechanisms underlying the assembly of intermediate filaments. *Exp. Cell Res.* **301**: 77–83.

Kreplak LaHB. 2008. Severe Myopathy Mutations Modify the Nanomechanics of Desmin Intermediate Filaments. *J. Mol. Biol.* **385**(4): 1043–1051.

Lacolley P, Challande P, Boumaza S, Cohuet G, Laurent S, Boutouyrie P, Grimaud J-A, Paulin D, Lamaziere J-MD, Li Z. 2001. Mechanical properties and structure of carotid arteries in mice lacking desmin. *Cardiovasc. Res.* **51**: 178–187.

Lazarides E. 1980. Intermediate filaments as mechanical integrators of cellular space. *Nature* **283**(5744): 249–256.

Ma L, Xu J, Coulombe PA, Wirtz D. 1999. Keratin filament suspensions show unique micromechanical properties. *J. Biol. Chem.* **274**: 19145–19151.

Meyer GA, Kiss B, Ward SR, Morgan DL, Kellermayer MSZ, Lieber RL. 2010. Theoretical prediction of the effect of force transmission by desmin on intersarcomere dynamics. *Biophys. J.* **98**: 258–266.

Milam L, Erickson HP. 1984. Structural characteristics of the desmin protofilament. *J. Ultrastruct. Res.* **89**: 179–186.

Mücke N, Kreplak L, Kirmse R, Wedig T, Herrmann H, Aebi U, Langowski J. 2004. Assessing the flexibility of intermediate filaments by atomic force microscopy. *J. Mol. Biol.* **335**(5): 1241–50.

Munoz-Marmol AM, Strasser G, Isamat M, Coulombe PA, Yang Y, Roca X, Vela E, Mate JL, Coll J, Fernandez-Figueras MT and others. 1998. A dysfunctional desmin mutation in a patient with severe generalized myopathy. *Proc. Natl. Acad. Sci. U.S.A.* **95**: 11312–11317.

Omary MB, Coulombe PA, McLean WH. 2004. Intermediate filament proteins and their associated diseases. *New Engl J Med* **351**: 2087–2100.

Osborn M. 1986. Intermediate filament proteins: a multigene family distinguishing major cell lineages. *Trends Biochem. Sci.* **11**(11): 469–472.

Parry DA. 2005. Microdissection of the sequence and structure of intermediate filament chains. *Adv. Protein Chem.* **70**: 113–142.

Pellissier JF, Pouger J, Charpin C, Figarell D. 1989. Myophaty associated with desmin type intermediare filaments. *Neurological science* **89**: 49–61.

Rivetti C, Guthold M, Bustamante C. 1996. Scanning force microscopy of DNA deposited onto mica: equilibration versus kinetic trapping studied by statistical polymer chain analysis. *J. Mol. Biol.* **264**(5): 919–32.

Sam M, Shah S, Friden J, Milner DJ, Capetanaki Y, Lieber RL. 2000. Desmin knockout muscles generate lower stress and are less vulnerable to injury compared with wild-type muscles. *Am. J. Physiol. Cell Physiol.* **279**(4): C1116-22.

Shah SB, Davis J, Weisleder N, Kostavassili I, McCulloch AD, Ralston E, Capetanki Y, Lieber RL. 2004. Structural and functional roles of desmin in mouse skeletal muscle during passive deformation. *Biophys. J.* **86**: 2993–3008.

Sharma SN, Mücke et al. 2009. Disease mutations in the "head" domain of the extra-sarcomeric protein desmin distinctly alter its assembly and network-forming properties. *J. Mol. Med.* **87** (12): 1207–1219.

Sjuve R, Arner A, Li Z, Mies B, Paulin D, Schmittner M, Small JV. 1998. Mechanical alterations in smooth muscle from mice lacking desmin. *J. Muscle Res. Cell Motil.* **19**(4): 415–29.

Steinert PM, Parry DA. 1985. Intermediate filaments: conformity and diversity of expression and structure. *Annu. Rev. Cell Biol.* **1**: 41–65.

Steinert PM, Jones JC, Goldman RD. 1984. Intermediate filaments. *J. Cell Biol.* **99**(1 Pt 2): 22s-27s.

Stromer MH, Ritter MA, Pang S, Robson RM. 1987. Effect of cations and temperature on kinetics of desmin assembly. *Biochem. J.* **246**: 75–81.

Stromer MH, Huiatt TW, Richardson RL, Robson RM. 1981. Disassembly of synthetic 10-nm desmin filaments from smooth muscle into protofilaments. *Eur. J. Cell Biol.* **25**(1): 136–43.

Wang N, Stamenovic D. 2003. Mechanics of vimentin intermediate filaments. In: Linke WA, Granzier HL, Kellermayer MSZ, editors. Mechanics of elastic biomolecules. Dordrecht: Kluwer Academic Publishers. p 535–540.